

Review Article

Open Access



# The neuromorphic computing for biointegrated electronics

Soon Joo Yoon<sup>1,#</sup>, Jin Tae Park<sup>1,#</sup>, Yoon Kyeong Lee<sup>1,2,\*</sup> 

<sup>1</sup>Department of Nano Convergence Engineering, Jeonbuk National University, Jeonju 54896, Republic of Korea.

<sup>2</sup>Division of Advanced Materials Engineering, Jeonbuk National University, Jeonju 54896, Republic of Korea.

<sup>#</sup>Authors contributed equally.

\*Correspondence to: Prof. Yoon Kyeong Lee, Division of Advanced Materials Engineering, Jeonbuk National University, 567, Baekje-daero, Deokjin-gu, Jeonju 54896, Republic of Korea. E-mail: yoonklee@jbnu.ac.kr

**How to cite this article:** Yoon SJ, Park JT, Lee YK. The neuromorphic computing for biointegrated electronics. *Soft Sci* 2024;4:30. <https://dx.doi.org/10.20517/ss.2024.12>

**Received:** 15 Mar 2024 **First Decision:** 7 May 2024 **Revised:** 4 Jul 2024 **Accepted:** 19 Jul 2024 **Published:** 16 Aug 2024

**Academic Editor:** YongAn Huang **Copy Editor:** Pei-Yun Wang **Production Editor:** Pei-Yun Wang

## Abstract

This review investigates the transformative potential of neuromorphic computing in advancing biointegrated electronics, with a particular emphasis on applications in medical sensing, diagnostics, and therapeutic interventions. By examining the convergence of edge computing and neuromorphic principles, we explore how emulating the operational principles of the human brain can enhance the energy efficiency and functionality of biointegrated electronics. The review begins with an introduction to recent breakthroughs in materials and circuit designs that aim to mimic various aspects of the biological nervous system. Subsequent sections synthesize demonstrations of neuromorphic systems designed to augment the functionality of healthcare-related electronic systems, including those capable of direct signal communication with biological tissues. The neuromorphic biointegrated devices remain in a nascent stage, with a relatively limited number of publications available. The current review aims to meticulously summarize these pioneering studies to evaluate the current state and propose future directions to advance the interdisciplinary field.

**Keywords:** Neuromorphic computing, biointegrated electronics, memristor, memtransistor

## INTRODUCTION

Recent strides in biointegrated electronics have significantly advanced our ability to monitor and interpret physiological activities within organs. Notable among these developments are bioimplants, including



© The Author(s) 2024. **Open Access** This article is licensed under a Creative Commons Attribution 4.0 International License (<https://creativecommons.org/licenses/by/4.0/>), which permits unrestricted use, sharing, adaptation, distribution and reproduction in any medium or format, for any purpose, even commercially, as long as you give appropriate credit to the original author(s) and the source, provide a link to the Creative Commons license, and indicate if changes were made.



multichannel electrocorticography (ECoG) devices and other technologies enabling real-time monitoring of brain activities<sup>[1,2]</sup>. Operating within the frequency range of approximately 1 kHz and across multiple channels, these implants offer deep insights into organ function, surpassing their initial role as simple biosignal measurement devices to encompass diagnostic capabilities and therapeutic interventions<sup>[3,4]</sup>. This paradigm shift in medical technology, exemplified by precise electrical stimulation to regulate abnormal neural activity, holds promise for personalized interventions in conditions such as epileptic seizures, benefiting patients with spinal and brain injuries<sup>[5-8]</sup>.

The integration of artificial intelligence (AI) technology with biointegrated devices enhances biosignal interpretation, propelling the field toward future medical care with real-time, targeted interventions. Despite these promising developments, challenges such as real-time processing and high-power consumption involved need to be addressed<sup>[9-11]</sup>. The energy demands of conventional bioimplants for physiological monitoring primarily stem from functions related to data acquisition, conversion, and transmission for further processing. Wireless communication to external processors, crucial for freely moving patients, often requires additional equipment to meet power supply needs. Alternative on-site processing can be beneficial in terms of reducing the response time and the amount of data communication. However, incorporating high-performance processors in implants raises other concerns about volume, mass, heat generation, and power supply. More advanced systems that provide intervention mechanisms further contribute to overall power requirements, underscoring the importance of energy-efficient design strategies.

Neuromorphic computing, inspired by the structure and function of the human brain, presents a natural alliance with such demands. The human brain's superior energy efficiency (~20 W) and performance in solving problems that require parallel or stochastic processing distinguishes it from conventional computers<sup>[12]</sup>. These remarkable capabilities stem from the unique structure of large-scale networks of neurons connected through synapses, enabling simultaneous data storage and processing with low power consumption. The communication mechanism between neurons in a biological neural network involves time-dependent spikes, contrasting with the logic-based computing process of the modern computers with von Neumann architecture. Neuromorphic hardware mimics these structural and communication features of the brain with various levels of abstraction using current-voltage (I-V) relationships of different electronic materials<sup>[13,14]</sup>.

This review comprehensively elucidates the scope of the implementation and application of neuromorphic computing for biointegrated electronics. It initiates with an overview of the concept of neuromorphic computing, providing a foundation for exploring various abstraction levels pertaining to the hardware implementation. Examples of neuromorphic systems capable of energy-efficient acquisition and analysis of healthcare-related data are presented, highlighting examples based on emerging memristive materials. The discussion extends to innovative devices and circuit designs, underscoring their significance in interpreting sensed signals from biology and aiding in disease diagnostics. Finally, the review addresses recent studies on neuromorphic devices that are integrated and communicate with biology, illustrating the potential for replacing biological neurons to cure diseases or enhance biological functionality. Despite being in the early stages of development, neuromorphic systems utilizing emerging materials and circuit designs are anticipated to progress towards more intricate architectures, significantly contributing to the intelligence of biointegrated healthcare systems.

## UNDERSTANDING THE RECENT EMERGENCE OF NEUROMORPHIC COMPUTING

The evolution of neuromorphic systems, serving as hardware abstractions of the brain, has become a focal point in recent research on electronic materials and devices. While the conventional approach to mimicking the brain has primarily involved benchmarking the algorithms used in brain processing, there is a growing interest in hardware that physically replicates the brain itself. This shift is partially driven by the necessity to accelerate the execution of artificial neural network (ANN) algorithms<sup>[15]</sup>. As the fields of computer science and neuroscience have advanced AI to a significant level, successful examples of ANNs have expanded into various domains, including natural language processing, image recognition, computer vision, autonomous vehicles, and other sectors, as demonstrated by AlphaGo and AlphaFold<sup>[16-21]</sup>. Nevertheless, the computational expenses associated with training ANNs and performing inference present a significant challenge with conventional central processing units (CPUs).

The major computational costs stem from the unoptimized serial processing of CPUs and the limited bandwidth for communication between processing and memory units, decelerating the speed of the computation, storage and loading of synaptic weights or other parameters in ANNs. Accelerators such as graphics processing units (GPUs) and neural processing units (NPUs), optimized for parallel processing, are actively utilized and under development to accelerate the computation with the aid of high-bandwidth memory (HBM) [Figure 1A]<sup>[22,23]</sup>. Additional efforts are directed towards reducing latency and energy consumption associated with fetching data from external memory by locating more memory in proximity to processors inside the same module, often referred to as process near memory (PNM)<sup>[24]</sup>.

An advanced approach eliminates the boundaries between memory and processors by incorporating the storage of relevant data into the physical state of processing units. In contrast to the traditional von Neumann architecture, where data storage and processing occur in physically separate locations, these novel efforts introduce the innovative concept of processing in memory (PIM) [Figure 1A]. The distributed memory structure in PIM where memory and logic devices are located on the same chip can be further advanced to resemble the brain's operations, where data undergo processing while moving across neurons (the processing element) through synapses (the memory element in the brain) in space. Such structure is called computing in memory (CIM) to distinguish it from PIM, but it is often presented as an advanced type of PIM in much of the literature.

The term “neuromorphic hardware” encompasses hardware that possesses the features of the brain distinguished from conventional computers at various levels and abstractions<sup>[25-28]</sup>. As previously mentioned, distributed memories and processors represent one of such distinguishing features. Other features pertain to event- or pulse-based signal communication during processing. Such hardware can be implemented using various electronic materials, with the most sophisticated demonstration achieved through silicon-based memory and logic devices<sup>[29]</sup>. Alternatively, emerging materials capable of processing analog data directly are also being explored, which will be discussed further in subsequent sections.

Despite variations in abstraction levels and applied materials and circuits, the anticipated advantages remain consistent. The overarching benefits expected from neuromorphic hardware encompass functions known to be inherently superior when executed by the brain compared to conventional computers. While computers excel in specific tasks requiring speed, accuracy, and large-scale repetitive data processing, the human brain remains superior in its capacity to execute a broad spectrum of cognitive functions with exceptional efficiency, adaptability, and creativity. Among these benefits, energy efficiency stands out as particularly noteworthy for edge computing for the devices with limited power sources.

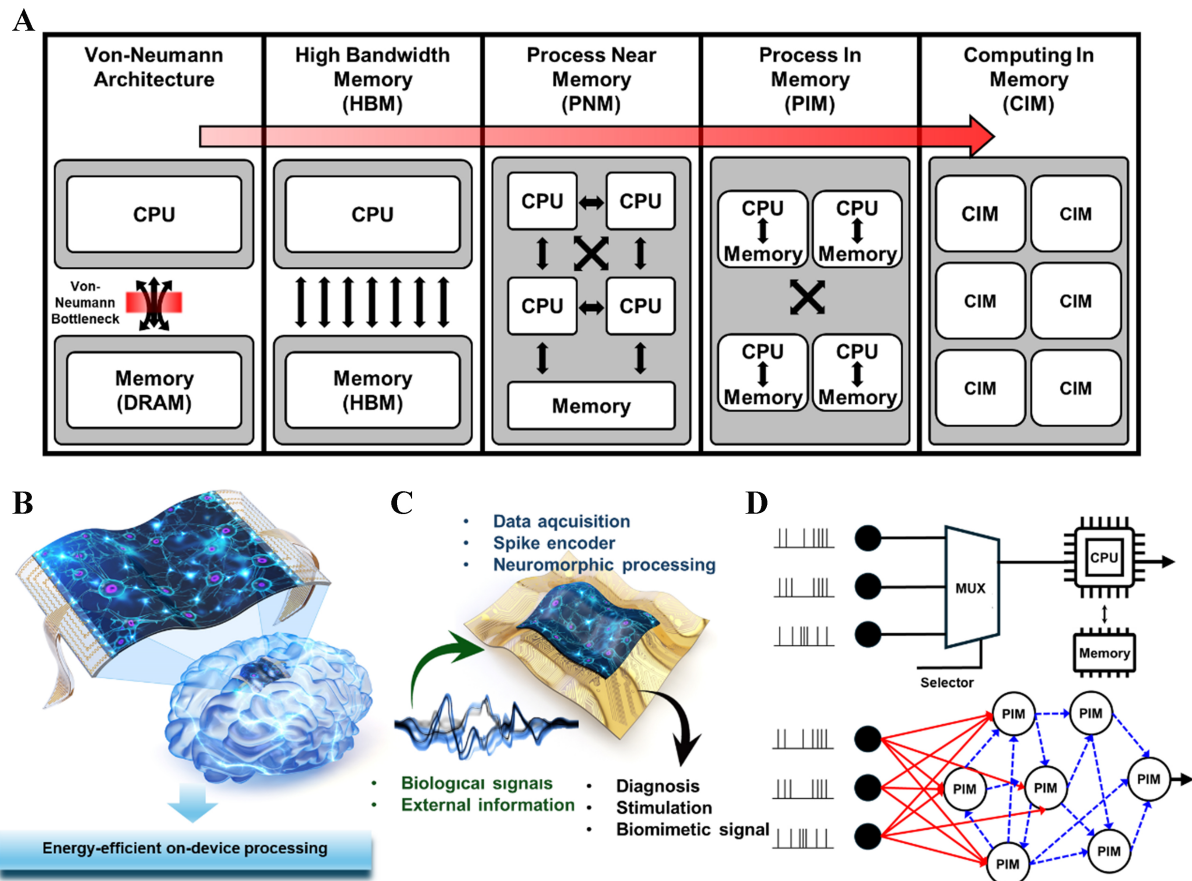


**Figure 1.** Advances in computing architectures and neuromorphic biointegrated electronics. (A) Schematic diagram illustrating conventional computing architectures and their evolution with advancements in data processing; (B) Schematic representation of biointegrated electronic systems designed for on-device neuromorphic computing; (C) The application of neuromorphic processing extends to transmitting external information to biological systems, processing biosignals for diagnostics, and facilitating therapeutic interventions; (D) Comparison between conventional (top) and neuromorphic (bottom) processing approaches.

## COMBINING NEUROMORPHIC COMPUTING WITH BIOINTEGRATED ELECTRONICS

Figure 1B illustrates the schematic representation of neuromorphic biointegrated electronic systems characterized by brain-like signal processing performed on-site. The integration of high-performance processors into conventional biointegrated systems raises concerns regarding heat generation and excessive power demand. Consequently, the functionality of conventional bioimplants is primarily confined to tasks associated with data acquisition, conversion, and transmission, particularly for facilitating wireless communication with external processors. Neuromorphic computing, inspired by the energy-efficient structure and function of the human brain, emerges as a promising solution to these challenges. By emulating the brain's intricate communication mechanisms within its dynamic network structure, neuromorphic systems hold the potential to enhance the functionality of the biointegrated systems that can extend to effectively conveying external information to biological entities or facilitating the acquisition and interpretation of biosignals [Figure 1C].

Figure 1D reveals the essential characteristics of neuromorphic computing systems by comparing with conventional processing approaches in managing continuously generated biopotentials sensed by multichannels of a biointegrated device. In the conventional system, a multiplexer (MUX) is employed for serial processing to accommodate numerous input signals, subsequently selecting and conveying the



necessary data for output. An amplifier is simultaneously integrated with the output to enhance information within predetermined bandwidth and temporal constraints. The acquired signal modifications are then processed by an analog-to-digital converter (A/D) and stored and processed in a separate computer with dedicated processors and memories for subsequent analysis<sup>[30]</sup>. This conventional approach to data processing is characterized by complexities leading to issues such as elevated energy consumption and diminished processing speed, especially when handling large datasets in parallel.

In contrast, neuromorphic computing is characterized by parallel processing of input data during signal transmission over time through physical space interconnected by distributed processing and memory elements<sup>[25,31,32]</sup>. PIM or CIM is a commonly employed term to delineate this processing paradigm, attributable to the processing occurring during signal transmission through those elements situated in close proximity<sup>[33]</sup>. Prior to delving into the specifics of biointegrated neuromorphic systems, the subsequent chapters provide a succinct overview of neuromorphic hardware from a broad perspective.

## PROCESSING IN THE BRAIN

The current trajectory of research in neuromorphic electronics is centered on the development of small-scale replications of specific components of the human brain rather than the complete emulation of the brain's integrative functionality. Since previous reviews have extensively covered the structural organization of biological neurons and emulating unit devices, a brief description suffices here<sup>[34-38]</sup>.

Biological neurons, the fundamental units of the nervous system, consist of distinct anatomical components: dendrites, soma (cell body), and axons [Figure 2A]<sup>[39]</sup>. Dendrites function as receivers for input signals originating from neighboring neurons. The input signals are transmitted via synapses, the sites of contact between the axon terminal of the signal-sending (presynaptic) neuron and the dendrite terminal of the signal-receiving (postsynaptic) neuron [Figure 2B]. Synaptic strength, determined by factors such as the amount of neurotransmitter release and receptor sensitivity, plays a pivotal role in modulating the amplitude of the response of the receiving neuron. Subsequently, the received signals are transmitted to the soma. Here, the soma integrates incoming signals from its multibranched dendrites, undergoing a nonlinear processing phase when the cumulative input exceeds a predefined threshold. This process culminates in a voltage spike called an action potential featuring an amplitude of approximately 110 mV and a duration spanning 1 to 10 ms [Figure 2C]. The action potentials are then conveyed to other neurons through axonal pathways<sup>[40]</sup>.

The integrate and fire (IF) model captures the firing event of neurons. In the circuit model of IF, the capacitor (C) discharges accumulated charges when the potential developed across the capacitor ( $V_{mem}$ ) exceeds a certain threshold. Figure 2D shows an example of such a circuit that utilizes a volatile threshold switch (TS) for the discharging process. This firing mechanism effectively captures the precise moment when an event of reaching the threshold voltage occurs. Inclusion of a leaky element in the circuit demonstrates leaky IF (LIF) model that can simulate the returning dynamics to the resting potential during the period without input signals. The IF or LIF model assumes that the specific shape of the spike holds minimal significance in processing information. Recent studies demonstrate advanced neuron models using supplementary circuits and rich dynamics of memristors to simulate neuronal memory effects such as adaptation and bursting<sup>[41,42]</sup>.

In addition to the IF model, the Hodgkin-Huxley (HH) model demonstrates a more detailed biophysical process of generating action potentials by explicitly incorporating circuit components to simulate the ionic current flow across the cell membrane. The HH model consists of several variable resistors and voltage

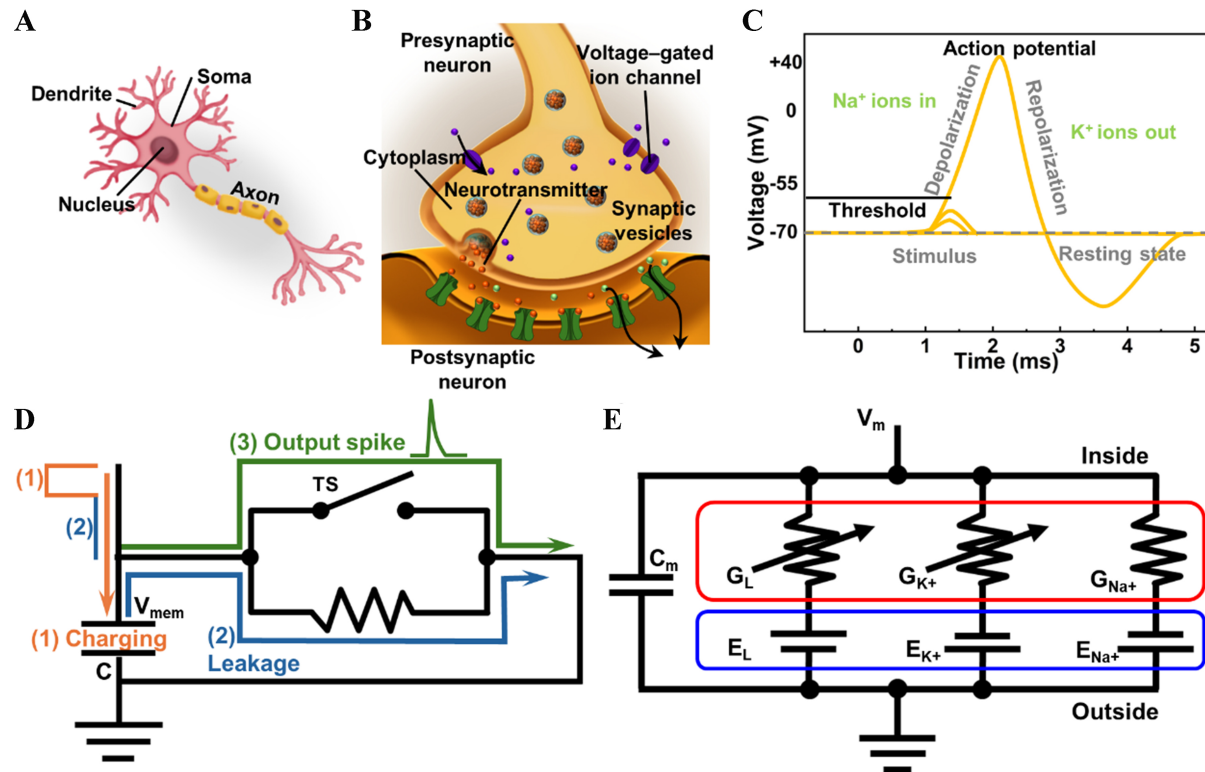


**Figure 2.** Biological neurons and artificial neuron model for neuromorphic computing. (A) Components of biological neurons; (B) Synapse as the site of transmission of electric and chemical signals between two neurons; (C) Membrane potential changes and the generation of action potential; (D) Circuit diagram of a LIF model, implemented using a capacitor, resistor, and TS; (E) HH model. The membrane potential ( $V_m$ ) of the circuit is determined by the conductance of variable resistors that represent ion channels. LIF: Leaky integrate and fire; TS: threshold switch; HH: Hodgkin-Huxley.

sources that correspond to the ion channels with different resting potentials to elucidate the membrane potential changes [Figure 2E]. The node voltage ( $V_m$ ) across the capacitor ( $C_m$ ) varies according to the changes in the conductance of  $\text{Na}^+$  and  $\text{K}^+$  channels ( $G_{\text{Na}^+}$ ,  $G_{\text{K}^+}$ ). The HH model can be advanced to include adaptation variables and stochasticity. However, the computer simulation of a large network composed of the HH model demands increased computational costs due to the high complexities involved in nonlinear dynamics of the components<sup>[43]</sup>. Building hardware that utilizes electronic circuits that physically reproduce the dynamics of biological neurons can provide potential solutions to these challenges<sup>[34,44-47]</sup>.

## EMERGING MATERIALS FOR NEUROMORPHIC COMPUTING

Modulation of membrane potential is critical in neuromorphic hardware that aims to mimic neuronal signal processing. Current research endeavors are focused on physically simulating the signal processing mechanisms of the neurons by utilizing various components including capacitors, resistors, TSs, and complementary metal-oxide-semiconductor (CMOS) technologies<sup>[48-52]</sup>.

Among various options for electronic components in these hardware-level simulations, the CMOS technology is capable of supporting the most sophisticated demonstrations of neuromorphic computing due to its advanced design and fabrication capabilities<sup>[53-55]</sup>. However, implementing neuronal dynamics in such digital devices presents challenges, requiring intricate configurations of components. For example, a spiking neural network (SNN) incorporating spike-timing-dependent plasticity (STDP), a well-known learning mechanism of SNNs, necessitates approximately 32 CMOS transistors per synapse<sup>[41,56-60]</sup>.

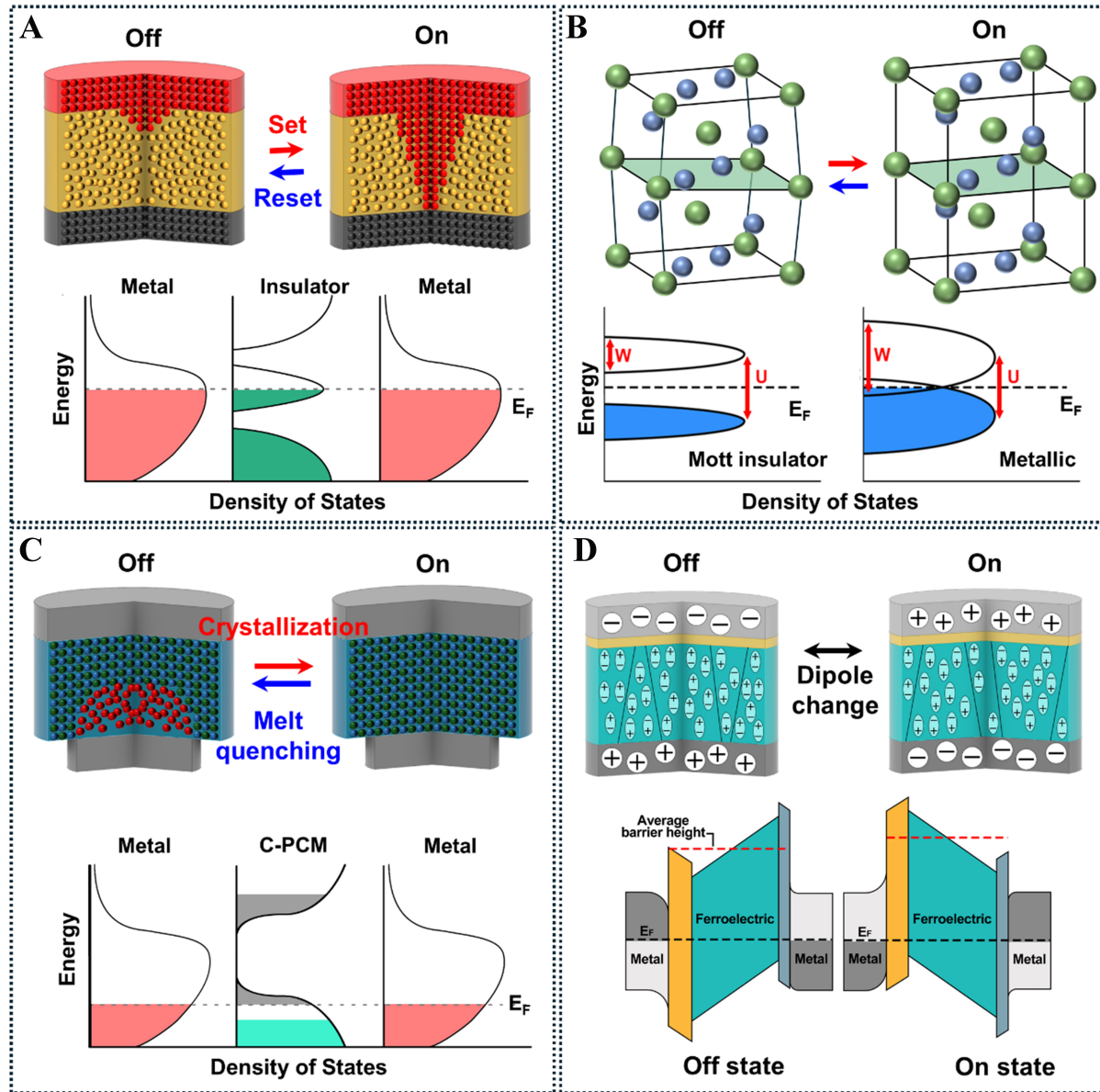
In this context, memristors emerge as promising candidates for neuromorphic computing owing to their characteristic history-dependent, analog-type physical states, beneficial for demonstrating the rich dynamics of neurons. Figure 3 illustrates representative emerging memristive devices that are often adopted for neuromorphic computing<sup>[41,59,61,62]</sup>. These devices can exhibit different resistance states, which depend on the formation of a conductive filament inside a high-resistance dielectric layer or the formation of a highly resistive phase inside a low-resistance surrounding phase<sup>[63]</sup>. Other materials with ferroelectric or magnetic properties have been utilized as memristive components in neuromorphic hardware. In this section, we will briefly overview the operation mechanisms of various types of resistive switching materials that are actively utilized for neuromorphic computing<sup>[64]</sup>.

Figure 3A describes resistance changes induced by electrical bias at metal-insulator-metal junctions through the migration of charged ions or vacancies influenced by electrochemical potential and temperature gradients<sup>[65]</sup>. For example, memristors can be implemented through redox reactions between electrodes using electrochemically active metals such as Ag and Cu. In this mechanism, metal cations oxidized at the interface migrate into the solid electrolyte and reduce at the opposite electrode, forming nuclei that grow into metal filaments. The formation of metallic filaments in various dielectric layers has been demonstrated through a scanning tunneling microscope and energy-dispersive X-ray spectroscopy<sup>[66-69]</sup>. Redox-based memristors often use amorphous insulators, which, in their OFF state, contain local electronic states bounded by mobility edges. These states facilitate thermal transfer mechanisms such as electron hopping. When subjected to external electric fields and heat, the stoichiometry of the amorphous insulator deviates due to redox reactions, leading to the formation of overlapping impurity orbitals. These localized impurity states form a non-localized impurity band, similar to a heavily doped amorphous semiconductor, thereby becoming conductive.

Recently, significant research activity has been focused on transistors and electronic devices based on the oxides of V or Nb. According to classical band theory, the Mott insulator is predicted to be a conductor; however, in practice, the band is separated due to the repulsion between electrons in the d and f orbitals, with the Fermi energy located between the band gaps. When external stress is applied, lattice deformation occurs, leading to band bending and enabling control of the band gap [Figure 3B]<sup>[64]</sup>. This ability to adjust the band gap not only allows for effective control but also enables the material to become conductive, making it suitable for a variety of electronic devices<sup>[70]</sup>.

The operating principle of phase change memory (PCM) relies on the thermally induced phase transition of the material. The atomic structure transforms from a disordered amorphous state with high resistance to a crystalline state with lower resistance, thus acting as a memory through changes in resistance. The PCM memristor generates heat due to the Joule effect between the electrodes, altering the crystal structure of the phase change layer [Figure 3C]. The OFF state of PCM-based memristors is generally amorphous with high crystallographic disorder, generating many localized electronic fields with exponentially decreasing wave functions<sup>[65]</sup>. This localization state, divided by mobility edges, fixes the Fermi level within the bandgap, reducing electrical conductivity. In the crystalline ON state, increased crystallinity through annealing creates a higher mobility edge. Additionally, chalcogenide element vacancies lower the Fermi level to the valence band, increasing carrier concentration and electrical conductivity.

Ferroelectric materials, exhibiting reversible remanent polarization, can change the dipole moment inside the material under an external electric field. This polarization state has been utilized in ferroelectric random access memory (FeRAM) due to its bit-encoding capability. Recent developments have highlighted ferroelectric material-based memristors as promising components for neuromorphic computing



**Figure 3.** Example of memristive materials. Operational principles and band diagrams of (A) ReRAM, (B) Mott insulator, (C) PCM, and (D) Ferroelectric memristor. (B) Reproduced with permission Copyright 2017, Nature Communications<sup>[64]</sup>. (A, C, D) Reproduced with permission Copyright 2020, Nature Communications<sup>[65]</sup>. ReRAM: Resistive random access memory; PCM: phase change memory.

applications. Memristors based on ferroelectric tunnel junctions (FTJs) consist of a metal-non-ferroelectric-ferroelectric-metal structure, where switched polarization alters the tunneling barrier and electron tunneling resistance [Figure 3D]. The electric field changes the direction and magnitude of the dipole within the ferroelectric, modifying the energy band structure and thereby the tunneling barrier and electron tunneling resistance<sup>[65]</sup>. The polarization dependence of the tunneling barrier is influenced by the ferroelectric-electrode interface, with asymmetry arising from differences in the thickness of the non-ferroelectric interfacial layer (yellow layer in Figure 3D) and the screening performance of the electrode.

## TWO-TERMINAL NEUROMORPHIC DEVICES

The physical states of memristors can be modulated by adjusting both the amplitude and timing of spike signals, facilitating the implementation of a synapse, and leading to reduced power consumption during both information storage and processing. Memristors offer rapid read and write operations with a simple two-terminal architecture, and various data retention characteristics depending on materials and operation scheme<sup>[71,72]</sup>. Figure 4A presents the representative I-V characteristics of memristive devices. The top plot depicts an I-V curve of volatile resistance switching, often referred to as threshold switching. The characteristic of the TS is the volatility of the low-resistance state after the voltage bias is removed across the memristive layer. The threshold voltages that cause switching to the low-resistance (ON) state and the return to the high-resistance (OFF) state often differ. The former voltage is termed the threshold voltage ( $V_{th}$ ), while the latter is termed the holding voltage ( $V_h$ ). The volatile switch is frequently employed to illustrate the dynamics of neurons, as its characteristic behavior of conducting current above the threshold and subsequently returning to the original state effectively demonstrates the firing of action potential and subsequent returning to a rest state.

The bottom curve of Figure 4A describes I-V characteristics of nonvolatile resistance switching. Devices with this characteristic are called bipolar switches, as the switching to low- (SET) and high-resistance (RESET) occurs upon applying opposite bias polarity. The resistance state after switching is nonvolatile without external bias once the state is achieved. The nonvolatile switch is utilized to describe the long-term memory of the synapse. However, the classification between volatile and nonvolatile switches can sometimes be ambiguous, as the retention time of the state without bias spans a wide range of times. Retention times below several seconds but longer than the period of the input signal pulses can induce hysteresis that can occasionally manifest complex dynamics of memory.

Numerous studies have investigated the effectiveness of hardware that operates computation during data flow through these volatile or nonvolatile memory devices. For example, integrating memristors in a crossbar array [Figure 4B] can capitalize on the resistance dependence of current output ( $I_{out}$ ) to perform matrix-vector multiplication<sup>[73]</sup>. In this setup, vectors are represented as input voltages ( $V_{in}$ ) to one electrode whereas matrix values are expressed as conductance values of a memristor ( $G$ ) located between the top and bottom electrodes. The measured output physically performs the multiplication ( $I_{out} = G \cdot V_{in}$ ). The two-terminal structure can be scaled up in large-scale crossbar arrays or random networks of nanowires [Figure 4B and C]<sup>[74-76]</sup>. Despite the accuracy limits stemming from non-idealities in analog-type processing through passive electronic devices, this approach offers promising solutions to mitigate the computational costs associated with training and inference in ANNs, as the operation maintains a constant time complexity regardless of the scale of the computation<sup>[77-80]</sup>.

Various studies have demonstrated that two-terminal memristor devices can effectively emulate the leaky integration and firing processes, which are essential characteristics of biological neurons. Figure 4D shows the circuit diagram of an adaptive LIF (ALIF) neuron based on the two-terminal  $VO_2$  memristor. Each spike from the LIF part charges  $C_2$  and increases  $V_g$ . The impact of the gate voltage ( $V_g$ ) applied to  $M_3$  on the spike frequency is depicted in Figure 4E. When  $V_g$  is below the threshold voltage of  $M_3$ ,  $M_3$  remains off, and the spiking frequency remains constant within this range. However, once  $V_g$  exceeds this threshold,  $M_3$  turns on, leading to an increase in leakage current, which subsequently reduces the charging amount of  $C_1$ . This results in a decrease in membrane potential  $V_m$  and, consequently, a reduction in the spiking frequency. This indicates that the spiking frequency can be modulated by  $V_g$ . The study shows that the implementation of a LIF circuit typically involves various resistor-capacitor (RC) circuits in addition to the memristor.



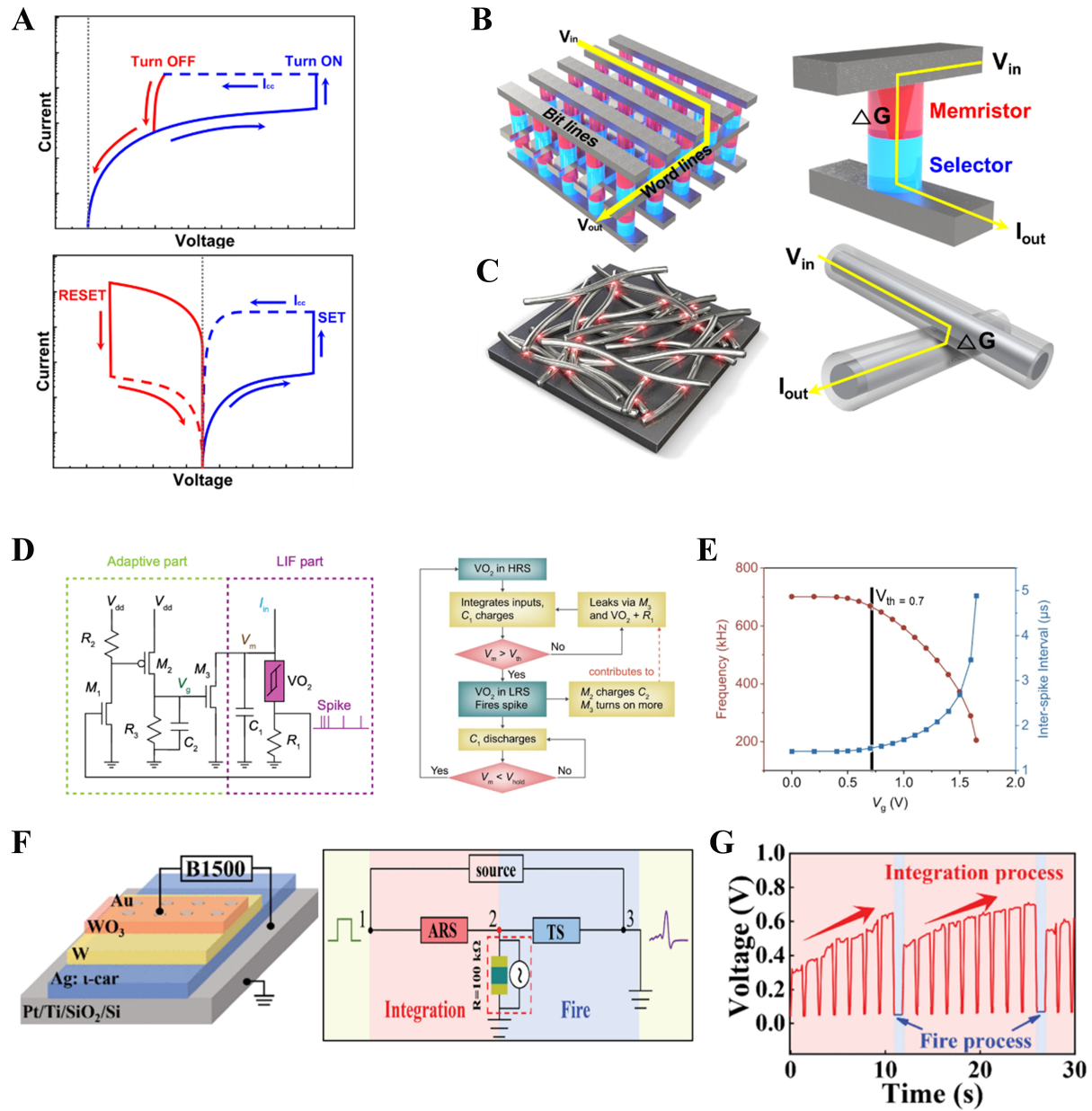


**Figure 4.** Two-terminal memristive devices and their implementation of LIF model. (A) Representative current-voltage (I-V) characteristics of volatile (top) and nonvolatile (bottom) memory devices; (B) Stacked 5 × 5 crossbar array utilizing memristive devices. The output current varies depending on the state of the memristor; (C) Schematic diagram of the nanowire-based memristor system used to implement the random network; (D) Circuit diagram of the  $\text{VO}_2$  memristor-based ALIF neuron; (E) Impact of  $V_g$  on the operational mechanism and spike frequency of ALIF neurons; (F) Schematic representation of a vertically stacked LIF device incorporating an analog resistive switching unit (ARS)-Threshold switching unit (W/Ag/Pt); (G) IF processes measured in the resistive component. (D and E) Reproduced with permission Copyright 2023, Nature Communications<sup>[70]</sup>. (F and G) Reproduced with permission Copyright 2022, IEEE Electron Device Letters<sup>[81]</sup>. LIF: Leaky integrate and fire; ALIF: adaptive LIF; IF: integrate and fire.

Figure 4F presents a LIF neuron device constructed exclusively with nonvolatile and volatile memristors<sup>[81]</sup>. The analog resistive switching (ARS) unit, constructed with Au/ $\text{WO}_x$ /W, exhibits nonvolatile characteristics, allowing its resistance to gradually decrease with the integration of input pulse voltage. Consequently, the voltage applied to the TS unit in series increases, eventually surpassing the threshold voltage and triggering a spike. Following this, the TS unit spontaneously reverts to a high resistance state



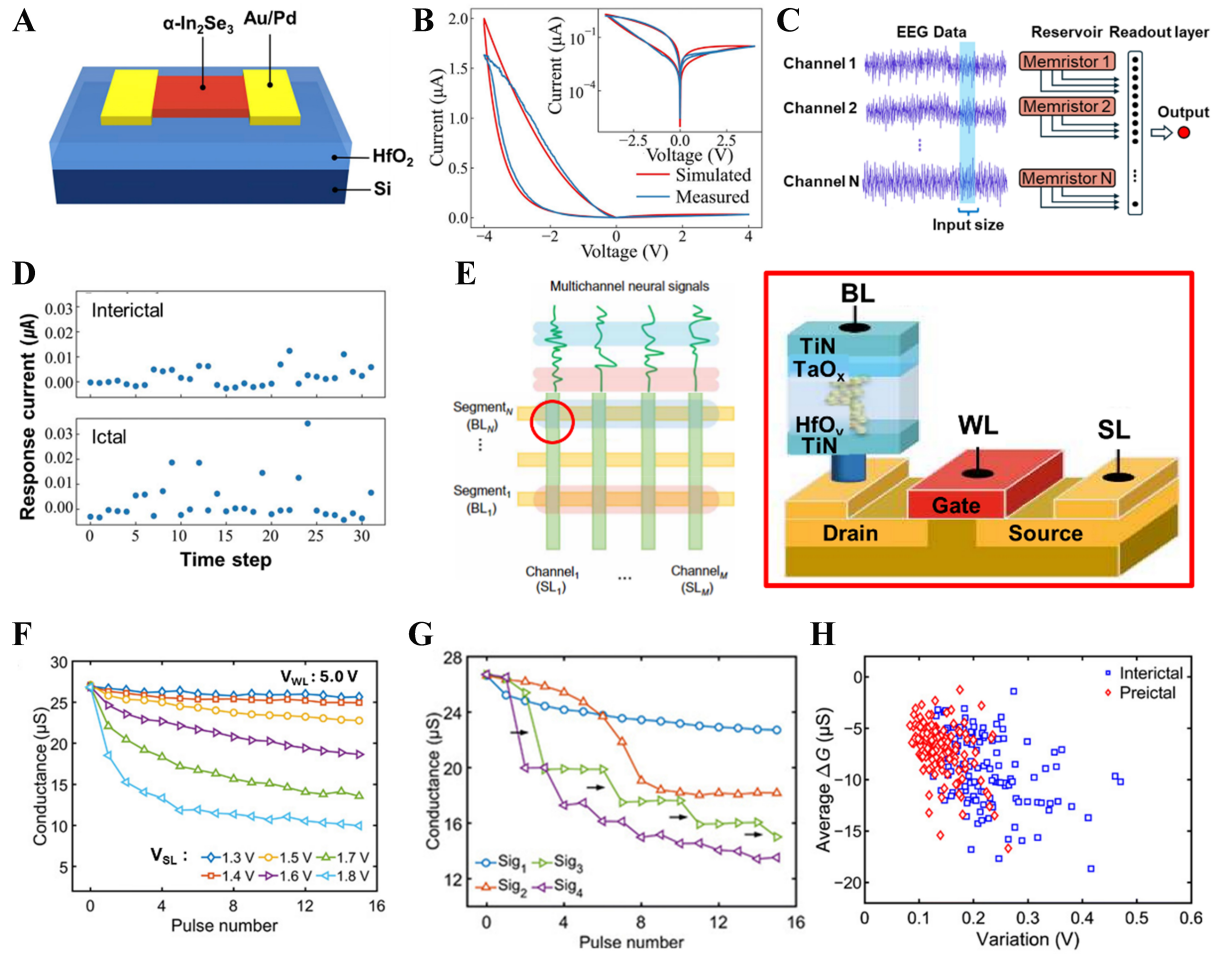
(HRS) within a brief period due to its volatile nature [Figure 4G].

Figure 5 summarizes recently published neuromorphic computing systems for electroencephalogram (EEG)-based epileptic seizure diagnostic systems. Figure 5A employs  $\alpha$ - $\text{In}_2\text{Se}_3$ -based dynamic memristor reservoir computing to streamline the training process<sup>[82]</sup>. The operating characteristics of the fabricated memristor were validated through the I-V transfer curve [Figure 5B]. The presence of a pinched hysteresis curve, which signifies memristive behavior, can be attributed to the ferroelectric properties of  $\text{In}_2\text{Se}_3$ . This behavior arises from the displacement of the Se atom situated at the center of the crystal structure.

The efficacy of the proposed system was validated through epileptic seizure prediction analyses conducted on EEG data procured from six patients. The data, representative of EEG signals acquired from 18 distinct scalp locations, was concurrently fed into a memristor array, serving as the input to the reservoir [Figure 5C]. Reservoir computing, characterized by its input layer, reservoir, and readout layers, significantly mitigates training overheads by necessitating training solely for the readout layer<sup>[83-85]</sup>. Furthermore, the integration of memristor technology, renowned for its PIM attributes, facilitates the development of compact, cost-efficient closed-loop systems. This approach underscores the potential of memristor-based reservoir computing in reducing the complexities and expenses associated with the training processes of diagnostic systems. The reservoir states correspond to the current output through the memristor. The upper panel of Figure 5D exhibits the 32 sampled response currents acquired from the interictal (non-seizure) input, whereas the lower panel showcases those obtained from the ictal (seizure) input. Notably, the ictal input data clip elicits a greater and accumulative response current compared to the interictal data, effectively capturing the temporal information embedded within the input data.

Another report presents an enhanced performance epileptic seizure detection system that processes intracranial electroencephalogram (iEEG) signals via a memristor array employing a 1T-1R (one transistor-one resistor) configuration. This system comprises 1k alternating arrays of  $\text{TiN}/\text{TaO}_x/\text{HfO}_y/\text{TiN}$  multilayer memristors; each memristor sits on top of the transistor drain terminal [bit line (BL)] [Figure 5E]<sup>[86]</sup>. The methodology for signal input involves the sequential transmission of the input signal across the word line (WL), segmenting it into equal lengths, and subsequently delivering these segments to the memristors situated in the corresponding row. This technique of signal division facilitates the temporal storage of information pertaining to the dynamically changing input signals within the memristor, thereby ensuring high accuracy. Notably, there exists a correlation between the amplitude of the input signal and the conductance change ( $\Delta G$ ) within the memristor, with an increase in signal amplitude prompting a significant augmentation in  $\Delta G$  [Figure 5F]. Figure 5G illustrates the conductance variation observed under various pulse patterns. The change in conductance ( $\Delta G$ ) correlates with both the amplitude of the input pulse and the subsequent pulse. This modulation of conductance enables precise encoding of signal wavelengths generated in the brain.

The system's efficacy was corroborated using pre- and post-seizure iEEG signals sourced from the Kaggle Seizure Prediction dataset as the input signals. The analysis revealed that despite similar signal energy and variation levels, the average  $\Delta G$  for preictal signals was markedly higher, thereby enabling precise seizure prediction [Figure 5H]<sup>[86]</sup>. These investigations affirmed the high compatibility of memristors with transistors used in conventional semiconductor devices, highlighting the potential for seamless integration within existing technological frameworks. The accuracy and sensitivity of the previous  $\alpha$ - $\text{In}_2\text{Se}_3$  and  $\text{TaO}_x/\text{HfO}_y$ -based computing showed higher performance compared to simple logistic regression method.



**Figure 5.** Neuromorphic computing for EEG-based seizure detection based on two-terminal devices. (A) Schematic of  $\alpha$ -In<sub>2</sub>Se<sub>3</sub>-based two-terminal memristor; (B) Current-voltage (I-V) characteristics of the device; (C) Process of computation involved in seizure detection within the system; (D) Current output from dynamic memristor from interictal and ictal data input. The ictal data clip showed a higher response current than the interictal data clip; (E) Crossbar array connected to multichannel sensors. Detailed structure of the 1T-1R memristor device (right); (F) Analog conductance modulation behaviors in RESET process for different  $V_{SL}$ ; (G) The average conductance change of 128 memristors in response to pulse train applications across different input signal waveforms; (H) Relationship between average  $\Delta G$  and signal energy across eight consecutive segments depending on the interictal or preictal states. (A-D) Reproduced with permission Copyright 2023, APL Machine Learning<sup>[82]</sup>. (E-H) Reproduced with permission Copyright 2020, Science Advances<sup>[86]</sup>. EEG: Electroencephalogram.

### THREE-TERMINAL NEUROMORPHIC DEVICES

While a two-terminal crossbar array architecture enables simple device integration and matrix calculation, the configuration inherently shares electrodes during the read-write process, resulting in unavoidable leakage currents and subsequent errors during the programming of synaptic weights<sup>[87-89]</sup>. In contrast, a synaptic device with three or more numbers of terminals employs a gate electrode that acts as a switch to control the channel conductance between the source and drain, enabling more accurate programming by allowing independent control of presynaptic and postsynaptic signals<sup>[90,91]</sup>.

Figure 6A-C illustrates a schematic diagram of an artificial visual sensory neuron implemented using a GeSe<sub>2</sub>-based three-terminal ovonic threshold switching (OTS) device<sup>[92]</sup>. OTS materials exhibit threshold switching through carrier trap-hopping by valence-alternating pairs (VAP) found in amorphous chalcogenide materials<sup>[93,94]</sup>. Initially, the application of a positive gate voltage causes Ag<sup>+</sup> ions to migrate

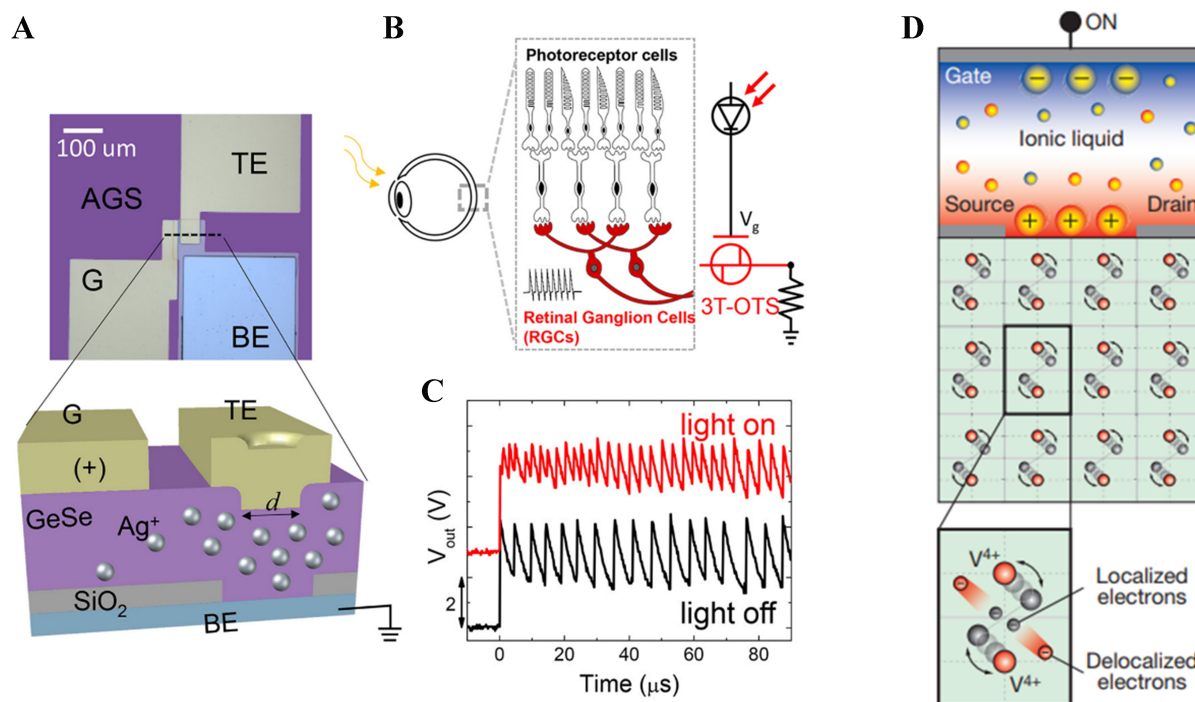


**Figure 6.** Three-terminal neuromorphic devices. (A) Optical micrograph of the OTS device and transport mechanism; (B) Schematic diagram comparing biological RGCs and artificial RGCs; (C) Output spike measured from the device connected in series with a resistor ( $V_{ds} = 5$  V). Change in device output with and without illumination; (D) Schematic of an electric double-layer transistor based on  $VO_2$ . (A–C) Reproduced with permission Copyright 2022, Nano Letters<sup>[92]</sup>. (D) Reproduced with permission Copyright 2012, Nature<sup>[95]</sup>. OTS: Ovonic threshold switching; RGCs: retinal ganglion cells.

near the bottom electrode in the Ag-doped  $GeSe_2$  layer, acting as a trap source and reducing the distance between hopping sites, facilitating the Poole-Frenkel transport. Additionally, the capacitance decreases as the gate voltage becomes more negative, indicating charge redistribution induced by  $V_g$ .

An artificial neuron was implemented by connecting the OTS element and a resistor ( $R_{OTS,ON} < R < R_{OTS,OFF}$ ) in series, and subsequently examining the spike characteristics. When an external voltage is applied to  $V_g$  in the OTS in the off state,  $V_{ds}$  increases due to the parasitic capacitance of the OTS. Once  $V_{ds}$  exceeds  $V_{th}$ , the device transitions to the on state, producing a spike. As the gate voltage increases, the spike frequency also grows (200~400 kHz), which is analogous to the behavior of biological neurons. Utilizing this property, an artificial visual sensory neuron was constructed by connecting a photoelectric diode to the gate electrode. It was observed that the spike frequency approximately doubled when the light was activated [Figure 6C].

Figure 6D shows an electric-double-layer transistor (EDLT) involving a  $VO_2$  channel and an organic ionic liquid that can induce the surface charge density of the channel up to  $10^{15} \text{ cm}^{-2}$ <sup>[95]</sup>. Electronic and structural phase transitions occur simultaneously owing to collective electron-lattice interactions at different temperatures depending on gate voltages ( $V_g$ ). Metal-insulator transition temperatures decrease dramatically with applied gate voltages above 0.3 V, indicating that the bulk region has been induced to enter the metallic state.

**Figure 7A** presents an approach utilizing organic electrochemical transistors (OECTs) based on organic mixed ion-electron conductors. OECTs emulate biological systems through their soft nature and ability to interact directly with ions in aqueous electrolytes<sup>[96]</sup>. Additionally, OECTs can function as either P-type or N-type depending on the channel material, enabling them to meet diverse requirements and exhibit high usability<sup>[97-100]</sup>. This versatility makes them highly adaptable for a range of applications. Initially, the input voltage pulse ( $V_g$ ) mobilizes ions within the ion gel, doping the channel and altering its conductance, resulting in a postsynaptic current<sup>[99]</sup>. When the voltage pulse is removed, the ions within the ion gel return to equilibrium, causing the postsynaptic current to gradually decrease.

**Figure 7B** illustrates the circuit diagram of a neuromorphic device constructed with P-type OECTs. In this configuration,  $T_1$  [poly(3,4-ethylenedioxythiophene):poly(styrene sulfonate) (PEDOT:PSS) channel] and  $T_2$  {poly(2-(3,3'-bis(2-(2-(2-methoxyethoxy)ethoxy)ethoxy)-[2,2'-bithiophen]-5-yl) thieno [3,2-b] thiophene) [p(g2T-TT)] channel} operate in depletion and enhancement modes, respectively<sup>[96]</sup>. Both the channel and the gate of the OECTs are in direct contact with the electrolyte. When a positive gate voltage ( $V_g$ ) is applied, positive ions migrate into the polymer channel, reducing the hole concentration [**Figure 7C**]. Various driving methodologies of OECTs can emulate the excitation-inhibition dynamics observed in neural networks, making them suitable for diverse biointegrated neuromorphic systems. Moreover, the imperative for wearable and implantable electronic devices necessitates materials that are flexible, adherent to the skin, and capable of accommodating physical deformations. OECTs, predominantly composed of organic polymers and flexible nanowires, fulfill these criteria and have found application in a wide array of biointegrated electronic devices.

**Figure 7D** illustrates a schematic representation of stretchable OECTs utilizing poly(3-hexylthiophene) (P3HT)/polyethylene oxide (PEO) nanowires, where a poly(vinylidene fluoride-co-hexafluoropropylene) (PVDF-HFP)/1-Ethyl-3-methylimidazolium bis(trifluoromethanesulfonyl)imide (EMIM-TFSI)-based ion gel adheres to a stretchable P3HT/PEO nanowire channel fabricated via electrospinning on a pliable silicone rubber substrate<sup>[101]</sup>. The synaptic behavior of these stretchable OECTs in response to presynaptic voltage spikes to the ion gel is analyzed in **Figure 7E**. Notably, the applied tensile strain elongates the channel, thereby attenuating the postsynaptic current output. Leveraging these characteristics, the extent of deformation can be quantified using postsynaptic currents, enabling precise detection of finger movements with high accuracy [**Figure 7F**]. The postsynaptic current and stretching velocity of the stretchable motion sensor, evaluated through finger gestures collected from three subject [**Figure 7G**]. This study demonstrates the potential of developing hardware-based ANNs capable of interacting with biological tissues, offering promising applications in biomonitoring and biosignal analysis.

## ORGANIC ELECTROLYTE TRANSISTORS BASED BIOINTEGRATED NEUROMORPHIC SYSTEMS

In biological systems, peripheral afferent nerves convey sensory information to the brain, while peripheral efferent nerves transmit stimulation signals from the brain to other parts of the body, crucial for muscle contraction and relaxation<sup>[102]</sup>. Disruptions to this intricate nervous network can severely affect basic motor functions. Neuroprosthetics, involving the replacement of damaged nervous and sensory organs with electronic devices, hold considerable promise in addressing various nerve-related disorders. Successful implementation of biointegrated neuroprosthetics requires incorporating sensing or motor elements capable of signal processing within their architecture, with input and output designed to emit pulse-based signals similar to biology to ensure compatibility in signal communication.



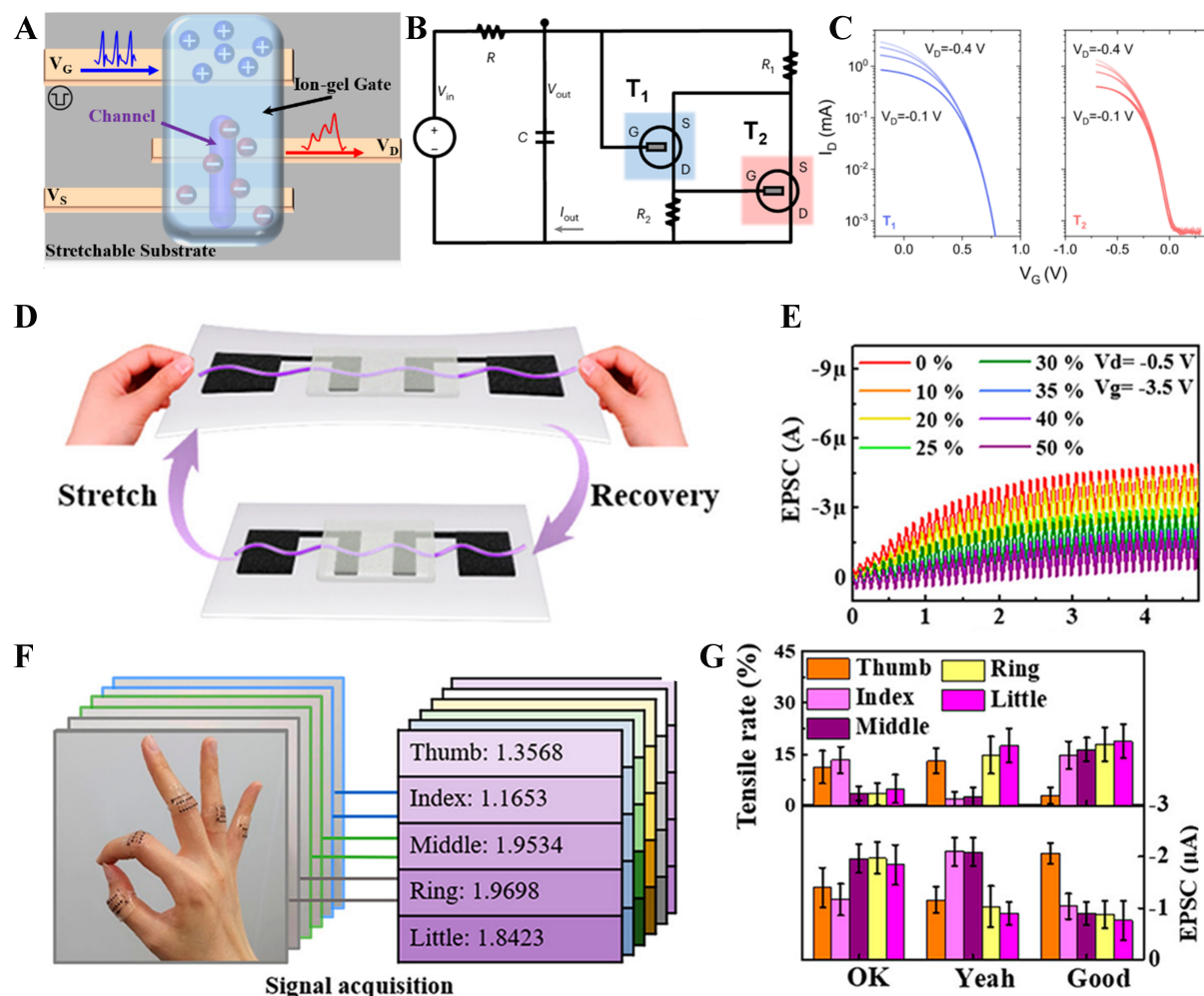


**Figure 7.** Schematic diagram of a neuromorphic system based on OEETs. (A) Schematic diagram illustrating the working mechanism of an electrolyte gate transistor; (B) Circuit diagram of an OAN, comprising two p-type OEETs ( $T_1$ ,  $T_2$ ) including an RC element; (C) Transfer curves of  $T_1$  (depletion mode) and  $T_2$  (enhancement mode) measured in the drain voltage range of 0.1 to 0.4 V; (D) Schematic illustration of the stretchable neuromorphic transistor; (E) Postsynaptic current of the device measured under tensile strain ranging from 0% to 50%; (F) Dataset of 270 hand shapes collected from a total of three individuals; (G) Tensile rate and postsynaptic current for hand gesture samples classified into three distinct motions. (B and C) Reproduced with permission Copyright 2022, Nature Electronics<sup>[96]</sup>. (D-G) Reproduced with permission Copyright 2022, ACS Nano<sup>[101]</sup>. OEETs: Organic electrochemical transistors; OAN: organic artificial neuron; RC: resistor-capacitor.

Artificial neurons based on memristors are gaining significant attention in the field of neuromorphic systems due to their high integration and accuracy. However, the susceptibility of solid memristor devices to moisture damage poses a challenge for their integration with living organisms, which have high moisture and ion concentrations. While research on biological signal processing before and after data acquisition by memristor arrays is active, their use for biointegrated real-time data analysis remains underdeveloped. The following study presents instances of neuromorphic devices seamlessly integrated with afferent and efferent nerve components, demonstrating the potential of bioimplantable closed-loop neuromorphic systems.

Artificial afferent nerves can convey the external information such as tactile stimulation, temperature, or other chemical environment to biology<sup>[103]</sup>. These biological sensory signals enable the performance of complex tasks by gathering information about the external environment [Figure 8A]<sup>[104]</sup>. While intricate

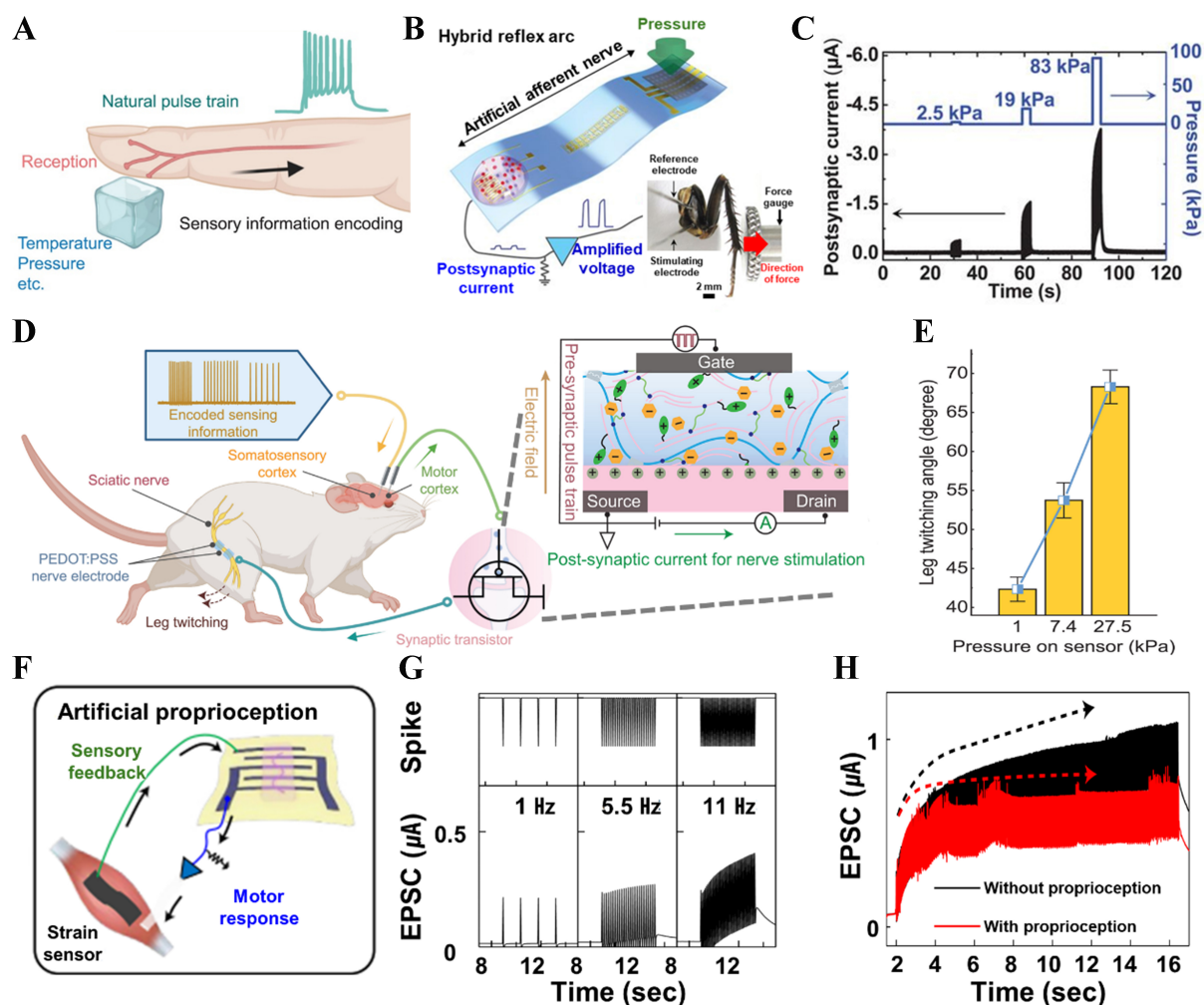


**Figure 8.** Biointegrated artificial afferent nerve and proprioception. (A) Schematic diagram illustrating the body's stimulus recognition process; (B) Schematic diagram of an OECT-based artificial afferent nerve integrated with a CNT-based pressure sensor and an organic ring oscillator; (C) Changes in postsynaptic current as a function of the intensity of applied pressure; (D) Schematic diagram of the artificial sensorimotor system; (E) Correlation between pressure and twitching angle measured in four rats; (F and G) The SNEN-based artificial proprioception. (F) The concept of artificial proprioception to recover voluntary motor function of a mouse through the use of SNEN (right). (G) Presynaptic gate voltage spikes and output drain current (EPSC) with frequencies from 1 to 11 Hz; (H) Comparison of EPSCs without proprioceptive feedback (black) and with proprioceptive feedback (red). (A, D, E) Reproduced with permission Copyright 2023, Science<sup>[104]</sup>. (B and C) Reproduced with permission Copyright 2018, Science<sup>[108]</sup>. (F-H) Reproduced with permission Copyright 2022, Nature Biomedical Engineering<sup>[111]</sup>. OECT: Organic electrochemical transistor; CNT: carbon nanotube; SNEN: stretchable neuromorphic efferent nerve; EPSC: excitatory postsynaptic current.

silicon circuits have been developed to emulate the peripheral nervous system and replicate biological skin-like perception, the construction of soft and deformable electronic skin (e-skin) using conventional Si-based circuits faces significant cost and material limitations<sup>[105]</sup>. Figure 8B shows that the pressure-sensitive synaptic device can be realized through the utilization of electrolyte gate transistors (EGTs) featuring multiple input gates in conjunction with a carbon nanotube (CNT) pressure sensor and a ring oscillator<sup>[106-108]</sup>. Upon application of a negative gate voltage, negative ions within the ion gel migrate in proximity to the channel, and induce subsequent turning on of the channel<sup>[109]</sup>. The electrical characteristics of the employed EGTs were scrutinized by examining their transfer curves. The lingering negative ions during the voltage sweep induce clockwise hysteresis, attributed to polarization effects.



The pressure-sensitive synaptic device operates by leveraging the responsiveness of the CNT pressure sensor, wherein an increase in pressure induces a corresponding reduction in the sensor's resistance owing to enhanced contact area. Concurrently, the applied pressure intensity modulates the input voltage of the ring oscillator, boosting the amplitude of the output voltage signal [Figure 8C]<sup>[108,110]</sup>. Subsequently, this pulse signal serves as the gate voltage input for the EGTs, thereby influencing the output drain current, akin to the postsynaptic current. Notably, the frequency of the output drain current tends to align with the frequency of the input pulse voltage. The intensity of the pressure applied to the sensor is proportional to the amplitude of the postsynaptic current, which is used to control the contractile force of the tibial flexor muscle in the discockroach leg according to the temporal and intensity characteristics of the applied pressure.

Figure 8D presents a schematic diagram of a biointegrated neuromorphic system implemented using stretchable synaptic transistors based on single-ion conducting polymer electrolyte {poly[(1-vinyl-3-propyl-imidazolium) bis(trifluoromethanesulfonyl)imide] (PiTFSI)}<sup>[104]</sup>. The synaptic behavior of the transistor was assessed via transfer curves under strain conditions of up to 50%, revealing the maintenance of a substantial hysteresis window. Initially, the pressure applied to the pressure sensor modulates its resistance, and the signal encoded through the ring oscillator integrated with the e-skin is conveyed to the somatosensory cortex of the rat, eliciting a feedback response in the motor cortex. The evoked motor signals traverse the artificial synapse, where they are summed and subsequently stimulate downstream muscles via the PEDOT:PSS electrode connected to the sciatic nerve, resulting in the contraction of the biceps femoris muscle. High-frequency voltage pulses stimulate the somatosensory cortex, and depending on the degree of stimulation, artificial postsynaptic currents induce leg movements in the rat within a range of 44.6° to 70.2°, successfully simulating a neuroprosthetic neuromorphic system [Figure 8E].

Existing neural prostheses that deliver the stimulation signals to the muscles often face limitations in their application to living bodies due to their high rigidity and power consumption, leading to non-physiological movements with rapid and unnatural muscle contractions and relaxations. Figure 8F presents the concept of stretchable neuromorphic efferent nerve (SNEN), designed to restore motor function by circumventing damaged neural pathways in the legs of mice afflicted with neuromotor impairments<sup>[111]</sup>. Synapse transistors, employing organic semiconductor nanowires as channels coupled with ion gel, demonstrate the ability to modulate channel conductivity by altering the concentration of anions near the channel in response to voltage pulses (action potentials)<sup>[112]</sup>. Notably, when applying action potentials with frequencies ranging from 5.5 to 11 Hz, surpassing the mobility rate of ions, a gradual increase in current at the drain electrode is observed, closely mimicking excitatory postsynaptic currents (EPSCs) and facilitating natural muscle movements [Figure 8G]. Furthermore, a CNT-based strain sensor with a resistance range of 100 kΩ to 3 MΩ adjusts the amplitude of the input pulse to the synapse transistor<sup>[113-115]</sup>. Consequently, modulation of the synapse transistor's input pulse according to the degree of muscle contraction and relaxation effectively mitigates the risk of muscle damage [Figure 8H]<sup>[111]</sup>.

## OUTLOOK

The advancements in diverse characteristics of emerging materials have catalyzed the development of neuromorphic computing systems that can be utilized for analyzing data generated from the biology. While these endeavors herald a promising convergence between neuromorphic computing and bio-related fields, it is imperative to acknowledge the inherent limitations of current technology.

Primarily, the presented research in disease diagnosis heavily relies on data from pre-existing repositories rather than direct acquisition from integrated sensors. As research progresses, a critical need arises for the

creation of devices endowed with integrated sensors capable of directly capturing biosignals. The authors contend that the application of neuromorphic computing to external devices with sufficient power sources may be limited, as such scenarios may prioritize processing methods that guarantee accuracy and speed. Leveraging the energy efficiency inherent in neuromorphic computing, on-site processing of biosignals becomes feasible, necessitating the integration of sensors and neuromorphic processing units within biointegrated devices. Also, the current trajectory of research predominantly emphasizes diagnostic capabilities over therapeutic interventions despite the commendable accuracy and cost-effectiveness demonstrated by neuromorphic-based systems in disease identification. Consequently, existing systems often require the transmission of results to external devices for further processing for treatment.

Other notable challenges persist regarding the chemical and mechanical compatibility between electronic and biological systems, as well as the unverified reliability of their operation in the biological environment<sup>[116-122]</sup>. For example, chalcogenide-based OTS is easily oxidized by the surrounding moisture<sup>[123]</sup>. Considering the biointegrated devices are in constant contact with biofluids, addressing the encapsulation issues is crucial for the practical application of neuromorphic computing for biointegrated systems.

The current neuromorphic systems have not yet achieved the scale and networking complexity of the human brain. The studies on biointegrated neuromorphic systems using emerging memristive materials are confined to simple electronic configurations composed of a small number of devices with limited scalability. While thin films are beneficial in fabricating flexible and stretchable devices, their current scale and sophistication levels fall short of conventional CMOS-based biochips or other medical apparatuses.

Discoveries in neuroscience suggest that many superior brain functions are attributed to the scale and network structure of the brain. The neuromorphic systems are anticipated to recognize and implement the importance of the specialized sub-parts of the brain interconnected on a large scale. Since advanced insights into the mechanisms involved in information processing provide valuable guidance for advancing biointegrated electronics, a close and continuous collaboration between engineering and neuroscience is essential for bridging the gap between current neuromorphic computing capabilities and the complexities of brain function. Addressing the aforementioned challenges and capitalizing on emerging opportunities, researchers are positioned to usher in a new era of advanced healthcare through the judicious integration of neuromorphic computing principles into medical devices.

## CONCLUSION

The advances in biointegrated electronics, exemplified by bioimplants and their integration with AI, mark the onset of a new era in personalized medical care. Despite these strides, challenges related to real-time processing and high-power consumption necessitate innovative solutions. Neuromorphic computing emerges as a promising ally, drawing inspiration from the human brain's efficiency and unique structural features. This review comprehensively explored the implementation and application of neuromorphic devices, showcasing their potential in achieving energy-efficient data acquisition, analysis, and disease diagnostics. More advanced forms of biointegrated systems demonstrated the potential for direct communication with biology to substitute or enhance the functionality of human body parts. Although systems utilizing emerging materials for neuromorphic systems are currently in the early stages of development, it is anticipated that these systems will evolve into more complex architectures, significantly contributing to the intelligence of embedded healthcare systems.

## DECLARATIONS

### Authors' contributions

Investigation, validation, data curation, visualization: Yoon SJ, Park JT  
Conceptualization, writing, supervision and funding acquisition: Lee YK  
All authors reviewed and commented on the manuscript before publication.

### Availability of data and materials

Not applicable.

### Financial support and sponsorship

This work was supported by the National Research Foundation of Korea (NRF) grant funded by the Korean government (Ministry of Science and ICT) (Nos. 2022R1C1C101007113, RS-2023-00221295).

### Conflicts of interest

Not applicable.

### Ethical approval and consent to participate

Not applicable.

### Consent for publication

Not applicable.

### Copyright

© The Author(s) 2024.

## REFERENCES

1. Dubey A, Ray S. Cortical electrocorticogram (ECoG) is a local signal. *J Neurosci* 2019;39:4299-311. [DOI](#) [PubMed](#) [PMC](#)
2. Alahi MEE, Liu Y, Xu Z, Wang H, Wu T, Mukhopadhyay SC. Recent advancement of electrocorticography (ECoG) electrodes for chronic neural recording/stimulation. *Mater Today Commun* 2021;29:102853. [DOI](#)
3. Yang T, Hakimian S, Schwartz TH. Intraoperative electrocorticography (ECog): indications, techniques, and utility in epilepsy surgery. *Epileptic Disord* 2014;16:271-9. [DOI](#) [PubMed](#)
4. Boran E, Ramantani G, Krayenbühl N, et al. High-density ECoG improves the detection of high frequency oscillations that predict seizure outcome. *Clin Neurophysiol* 2019;130:1882-8. [DOI](#) [PubMed](#)
5. Anwar H, Khan QU, Nadeem N, Pervaiz I, Ali M, Cheema FF. Epileptic seizures. *Discoveries* 2020;8:e110. [DOI](#) [PubMed](#) [PMC](#)
6. Shoeibi A, Khodatars M, Ghassemi N, et al. Epileptic seizures detection using deep learning techniques: a review. *Int J Environ Res Public Health* 2021;18:5780. [DOI](#) [PubMed](#) [PMC](#)
7. Assi E, Nguyen DK, Rihana S, Sawan M. Towards accurate prediction of epileptic seizures: a review. *Biomed Signal Proces* 2017;34:144-57. [DOI](#)
8. Amengual-Gual M, Sánchez Fernández I, Loddenkemper T. Patterns of epileptic seizure occurrence. *Brain Res* 2019;1703:3-12. [DOI](#) [PubMed](#)
9. Das R, Moradi F, Heidari H. Biointegrated and wirelessly powered implantable brain devices: a review. *IEEE Trans Biomed Circuits Syst* 2020;14:343-58. [DOI](#) [PubMed](#)
10. Koo JH, Song J, Yoo S, Sunwoo S, Son D, Kim D. Unconventional device and material approaches for monolithic biointegration of implantable sensors and wearable electronics. *Adv Mater Technol* 2020;5:2000407. [DOI](#)
11. Ray TR, Choi J, Bhandokar AJ, et al. Bio-integrated wearable systems: a comprehensive review. *Chem Rev* 2019;119:5461-533. [DOI](#) [PubMed](#)
12. Farkhani H, Tohidi M, Farkhani S, Madsen JK, Moradi F. A low-power high-speed spintronics-based neuromorphic computing system using real-time tracking method. *IEEE J Emerg Sel Topics Circuits Syst* 2018;8:627-38. [DOI](#)
13. Xia Q, Yang JJ. Memristive crossbar arrays for brain-inspired computing. *Nat Mater* 2019;18:309-23. [DOI](#) [PubMed](#)
14. Ielmini D, Wong HP. In-memory computing with resistive switching devices. *Nat Electron* 2018;1:333-43. [DOI](#)
15. Basheer IA, Hajmeer M. Artificial neural networks: fundamentals, computing, design, and application. *J Microbiol Methods* 2000;43:3-31. [DOI](#) [PubMed](#)
16. Chun J, Atalan E, Kim SB, et al. Rapid identification of streptomycetes by artificial neural network analysis of pyrolysis mass

- spectra. *FEMS Microbiol Lett* 1993;114:115-9. [DOI](#)
17. Chun J, Atalan E, Ward AC, Goodfellow M. Artificial neural network analysis of pyrolysis mass spectrometric data in the identification of *Streptomyces* strains. *FEMS Microbiol Lett* 1993;107:321-6. [DOI](#) [PubMed](#)
18. Timmins EM, Goodacre R. Rapid quantitative analysis of binary mixtures of *Escherichia coli* strains using pyrolysis mass spectrometry with multivariate calibration and artificial neural networks. *J Appl Microbiol* 1997;83:208-18. [DOI](#) [PubMed](#)
19. Goodacre R. Use of pyrolysis mass spectrometry with supervised learning for the assessment of the adulteration of milk of different species. *Appl Spectrosc* 1997;51:1144-53. [DOI](#)
20. Vallejo-cordoba B, Arteaga G, Nakai S. Predicting milk shelf-life based on artificial neural networks and headspace gas chromatographic data. *J Food Sci* 1995;60:885-8. [DOI](#)
21. Horimoto Y, Lee K, Nakai S. Classification of microbial defects in milk using a dynamic headspace gas chromatograph and computer-aided data processing. 2. Artificial neural networks, partial least-squares regression analysis, and principal component regression analysis. *J Agric Food Chem* 1997;45:743-7. [DOI](#)
22. Yazdanbakhsh A, Park J, Sharma H, Lotfi-Kamran P, Esmailzadeh H. Neural acceleration for GPU throughput processors. In: The 48th Annual IEEE/ACM International Symposium of Microarchitecture; 2015 Dec 05-09; Waikiki, Hawaii. Association for Computing Machinery; 2015. pp. 482-93. [DOI](#)
23. Tan T, Cao G. Efficient execution of deep neural networks on mobile devices with NPU. In: Proceedings of the 20th International Conference on Information Processing in Sensor Networks (Co-Located with CPS-IoT Week 2021); 2021 May 18-21; Nashville, USA. Association for Computing Machinery; 2021. pp. 283-98. [DOI](#)
24. She X, Long Y, Mukhopadhyay S. Improving robustness of ReRAM-based spiking neural network accelerator with stochastic spike-timing-dependent-plasticity. In: 2019 International Joint Conference on Neural Networks (IJCNN); 2019 Jul 14-19; Budapest, Hungary. IEEE; 2019. p. 1-8. [DOI](#)
25. Schuman CD, Kulkarni SR, Parsa M, Mitchell JP, Date P, Kay B. Opportunities for neuromorphic computing algorithms and applications. *Nat Comput Sci* 2022;2:10-9. [DOI](#) [PubMed](#)
26. Rajendran B, Sebastian A, Schmuker M, Srinivasa N, Eleftheriou E. Low-power neuromorphic hardware for signal processing applications: a review of architectural and system-level design approaches. *IEEE Signal Process Mag* 2019;36:97-110. [DOI](#)
27. Young AR, Dean ME, Plank JS, Rose GS. A review of spiking neuromorphic hardware communication systems. *IEEE Access* 2019;7:135606-20. [DOI](#)
28. Wan Q, Sharbati MT, Erickson JR, Du Y, Xiong F. Emerging artificial synaptic devices for neuromorphic computing. *Adv Mater Technol* 2019;4:1900037. [DOI](#)
29. Kornijczuk V, Jeong DS. Recent progress in real-time adaptable digital neuromorphic hardware. *Adv Intell Syst* 2019;1:1900030. [DOI](#)
30. Geng Z, Pepper MG, Yan Y. A multiplexer system for multi-channel charge signal processing in in-shoe force measurement. In: 2011 IEEE International Instrumentation and Measurement Technology Conference; 2011 May 10-12; Hangzhou, China. IEEE; 2011. p. 1-5. [DOI](#)
31. Davies M, Wild A, Orchard G, et al. Advancing neuromorphic computing with loihi: a survey of results and outlook. *Proc IEEE* 2021;109:911-34. [DOI](#)
32. Valle J, Ramirez JG, Rozenberg MJ, Schuller IK. Challenges in materials and devices for resistive-switching-based neuromorphic computing. *J Appl Phys* 2018;124:211101. [DOI](#)
33. Zou X, Xu S, Chen X, Yan L, Han Y. Breaking the von Neumann bottleneck: architecture-level processing-in-memory technology. *Sci China Inf Sci* 2021;64:3227. [DOI](#)
34. Ma J, Tang J. A review for dynamics in neuron and neuronal network. *Nonlinear Dyn* 2017;89:1569-78. [DOI](#)
35. Burkitt AN. A review of the integrate-and-fire neuron model: I. Homogeneous synaptic input. *Biol Cybern* 2006;95:1-19. [DOI](#) [PubMed](#)
36. Long L, Fang G. A review of biologically plausible neuron models for spiking neural networks. In: AIAA Infotech@Aerospace 2010; 2010 Apr 20-22; Atlanta, Georgia. American Institute of Aeronautics and Astronautics; 2010. [DOI](#)
37. Yamazaki K, Vo-Ho VK, Bulsara D, Le N. Spiking neural networks and their applications: a review. *Brain Sci* 2022;12:863. [DOI](#) [PubMed](#) [PMC](#)
38. Lansky P, Ditlevsen S. A review of the methods for signal estimation in stochastic diffusion leaky integrate-and-fire neuronal models. *Biol Cybern* 2008;99:253-62. [DOI](#) [PubMed](#)
39. Lee K, Silva BN, Han K. Deep learning entrusted to fog nodes (DLEFN) based smart agriculture. *Appl Sci* 2020;10:1544. [DOI](#)
40. Yang R, Huang H, Guo X. Memristive synapses and neurons for bioinspired computing. *Adv Elect Mater* 2019;5:1900287. [DOI](#)
41. Burr GW, Shelby RM, Sebastian A, et al. Neuromorphic computing using non-volatile memory. *Adv Phys X* 2017;2:89-124. [DOI](#)
42. Upadhyay NK, Jiang H, Wang Z, Asapu S, Xia Q, Joshua Yang J. Emerging memory devices for neuromorphic computing. *Adv Mater Technol* 2019;4:1800589. [DOI](#)
43. Shama F, Haghiri S, Imani MA. FPGA realization of hodgkin-huxley neuronal model. *IEEE Trans Neural Syst Rehabil Eng* 2020;28:1059-68. [DOI](#)
44. Liu Y, Iu HHC, Qian Y. Implementation of Hodgkin-Huxley neuron model with the novel memristive oscillator. *IEEE Trans Circuits Syst II* 2021;68:2982-6. [DOI](#)
45. Corinto F, Ascoli A, Sung-Mo SK. Memristor-based neural circuits. In: 2013 IEEE International Symposium on Circuits and Systems (ISCAS); 2013 May 19-23; Beijing, China. IEEE; 2013. pp. 417-20. [DOI](#)

46. Fang X, Duan S, Wang L. Memristive Hodgkin-Huxley spiking neuron model for reproducing neuron behaviors. *Front Neurosci* 2021;15:730566. DOI PubMed PMC
47. Xu Y, Gao S, Li Z, Yang R, Miao X. Adaptive Hodgkin-Huxley neuron for retina-inspired perception. *Adv Intell Syst* 2022;4:2200210. DOI
48. Yang Z, Han Z, Huang Y, Ye TT. 55nm CMOS analog circuit implementation of LIF and STDP functions for low-power SNNs. In: 2021 IEEE/ACM International Symposium on Low Power Electronics and Design (ISLPED); 2021 Jul 26-28; Boston, USA. IEEE; 2021. p. 1-6. DOI
49. Koshino S, Misawa N, Matsui C, Takeuchi K. Compact CiM co-optimized by heterogeneous multi-level ReRAM & random weight SNN for event-based vision sensor of edge AI. In: 2022 IEEE Silicon Nanoelectronics Workshop (SNW); 2022 Jun 11-12; Honolulu, USA. IEEE; 2022. p. 1-2. DOI
50. Luo J, Yu L, Liu T, et al. Capacitor-less stochastic leaky-FeFET neuron of both excitatory and inhibitory connections for SNN with reduced hardware cost. In: 2019 IEEE International Electron Devices Meeting (IEDM); 2019 Dec 07-11; San Francisco, USA. IEEE; 2019. pp. 6.4.1-6.4.4. DOI
51. Uleru GI, Hulea M. Influence of capacitor variability on the electronic spiking neurons. In: 2021 25th International Conference on System Theory, Control and Computing (ICSTCC); 2021 Oct 20-23; Iasi, Romania. IEEE; 2021. pp. 255-9. DOI
52. Radamson HH, Zhu H, Wu Z, et al. State of the art and future perspectives in advanced CMOS technology. *Nanomaterials* 2020;10:1555. DOI PubMed PMC
53. Rahiminejad E, Azad F, Parvizi-Fard A, Amiri M, Linares-Barranco B. A neuromorphic CMOS circuit with self-repairing capability. *IEEE Trans Neural Netw Learn Syst* 2022;33:2246-58. DOI
54. Basu A, Acharya J, Karnik T, et al. Low-power, adaptive neuromorphic systems: recent progress and future directions. *IEEE J Emerg Sel Topics Circuits Syst* 2018;8:6-27. DOI
55. Saxena V, Wu X, Zhu K. Energy-efficient CMOS memristive synapses for mixed-signal neuromorphic system-on-a-chip. In: 2018 IEEE International Symposium on Circuits and Systems (ISCAS); 2018 May 27-30; Florence, Italy. IEEE; 2018. p. 1-5. DOI
56. Iakymchuk T, Rosado-muñoz A, Guerrero-martínez JF, Bataller-mompeán M, Francés-villora JV. Simplified spiking neural network architecture and STDP learning algorithm applied to image classification. *J Image Video Proc* 2015;2015:59. DOI
57. Serrano-Gotarredona T, Masquelier T, Prodromakis T, Indiveri G, Linares-Barranco B. STDP and STDP variations with memristors for spiking neuromorphic learning systems. *Front Neurosci* 2013;7:2. DOI PubMed PMC
58. Debanne D, Inglebert Y. Spike timing-dependent plasticity and memory. *Curr Opin Neurobiol* 2023;80:102707. DOI PubMed
59. Wang R, Shi T, Zhang X, et al. Bipolar analog memristors as artificial synapses for neuromorphic computing. *Materials* 2018;11:2102. DOI PubMed PMC
60. Indiveri G, Chicca E, Douglas R. A VLSI array of low-power spiking neurons and bistable synapses with spike-timing dependent plasticity. *IEEE Trans Neural Netw* 2006;17:211-21. DOI
61. Wang R, Yang J, Mao J, et al. Recent advances of volatile memristors: devices, mechanisms, and applications. *Adv Intell Syst* 2020;2:2000055. DOI
62. Corinto F, Civalieri PP, Chua LO. A theoretical approach to memristor devices. *IEEE J Emerg Sel Topics Circuits Syst* 2015;5:123-32. DOI
63. Woo J, Moon K, Song J, et al. Improved synaptic behavior under identical Pulses using AlO<sub>x</sub>/HfO<sub>2</sub> bilayer RRAM array for neuromorphic systems. *IEEE Electron Device Lett* 2016;37:994-7. DOI
64. Li Z, Wu J, Hu Z, et al. Imaging metal-like monoclinic phase stabilized by surface coordination effect in vanadium dioxide nanobeam. *Nat Commun* 2017;8:15561. DOI PubMed PMC
65. Wang Z, Wu H, Burr GW, et al. Resistive switching materials for information processing. *Nat Rev Mater* 2020;5:173-95. DOI
66. Xu Z, Bando Y, Wang W, Bai X, Golberg D. Real-time *in situ* HRTEM-resolved resistance switching of Ag<sub>2</sub>S nanoscale ionic conductor. *ACS Nano* 2010;4:2515-22. DOI PubMed
67. Yuan F, Zhang Z, Liu C, et al. Real-time observation of the electrode-size-dependent evolution dynamics of the conducting filaments in a SiO<sub>2</sub> layer. *ACS Nano* 2017;11:4097-104. DOI PubMed
68. Yang Y, Gao P, Gaba S, Chang T, Pan X, Lu W. Observation of conducting filament growth in nanoscale resistive memories. *Nat Commun* 2012;3:732. DOI PubMed
69. Tian X, Yang S, Zeng M, et al. Bipolar electrochemical mechanism for mass transfer in nanoionic resistive memories. *Adv Mater* 2014;26:3649-54. DOI PubMed
70. Yuan R, Tiw PJ, Cai L, et al. A neuromorphic physiological signal processing system based on VO<sub>2</sub> memristor for next-generation human-machine interface. *Nat Commun* 2023;14:3695. DOI PubMed PMC
71. Chen W, Song L, Wang S, et al. Essential characteristics of memristors for neuromorphic computing. *Adv Elect Mater* 2023;9:2200833. DOI
72. Sun W, Gao B, Chi M, et al. Understanding memristive switching via *in situ* characterization and device modeling. *Nat Commun* 2019;10:3453. DOI PubMed PMC
73. Seok JY, Song SJ, Yoon JH, et al. A review of three-dimensional resistive switching cross-bar array memories from the integration and materials property points of view. *Adv Funct Mater* 2014;24:5316-39. DOI
74. Feng X, Li S, Wong SL, et al. Self-selective multi-terminal memtransistor crossbar array for in-memory computing. *ACS Nano* 2021;15:1764-74. DOI PubMed



75. Li Y, Ang K. Hardware implementation of neuromorphic computing using large-scale memristor crossbar arrays. *Adv Intell Syst* 2021;3:2000137. DOI
76. Kuncic Z, Nakayama T. Neuromorphic nanowire networks: principles, progress and future prospects for neuro-inspired information processing. *Adv Phys X* 2021;6:1894234. DOI
77. Lee YK, Jeon JW, Park ES, et al. Matrix mapping on crossbar memory arrays with resistive interconnects and its use in in-memory compression of biosignals. *Micromachines* 2019;10:306. DOI PubMed PMC
78. Li J, Ren SG, Li Y, et al. Sparse matrix multiplication in a record-low power self-rectifying memristor array for scientific computing. *Sci Adv* 2023;9:eadf7474. DOI PubMed PMC
79. Woods W, Teuscher C. Approximate vector matrix multiplication implementations for neuromorphic applications using memristive crossbars. In: 2017 IEEE/ACM International Symposium on Nanoscale Architectures (NANOARCH); 2017 Jul 25-26; Newport, USA. IEEE; 2017. pp. 103-8. DOI
80. Bao H, Zhou H, Li J, et al. Toward memristive in-memory computing: principles and applications. *Front Optoelectron* 2022;15:23. DOI PubMed PMC
81. Bian J, Tao Y, Wang Z, et al. A stacked memristive device enabling both analog and threshold switching behaviors for artificial leaky integrate and fire neuron. *IEEE Electron Device Lett* 2022;43:1436-9. DOI
82. Yang Z, Liu K, Yuan R, et al. Seizure detection using dynamic memristor-based reservoir computing and leaky integrate-and-fire neuron for post-processing. *APL Mach Learn* 2023;1:046123. DOI
83. Moon J, Ma W, Shin JH, et al. Temporal data classification and forecasting using a memristor-based reservoir computing system. *Nat Electron* 2019;2:480-7. DOI
84. Du C, Cai F, Zidan MA, Ma W, Lee SH, Lu WD. Reservoir computing using dynamic memristors for temporal information processing. *Nat Commun* 2017;8:2204. DOI PubMed PMC
85. Zhong Y, Tang J, Li X, Gao B, Qian H, Wu H. Dynamic memristor-based reservoir computing for high-efficiency temporal signal processing. *Nat Commun* 2021;12:408. DOI PubMed PMC
86. Liu Z, Tang J, Gao B, et al. Multichannel parallel processing of neural signals in memristor arrays. *Sci Adv* 2020;6:eabc4797. DOI PubMed PMC
87. Abbas H, Abbas Y, Truong SN, et al. A memristor crossbar array of titanium oxide for non-volatile memory and neuromorphic applications. *Semicond Sci Technol* 2017;32:065014. DOI
88. Fernando BR, Qi Y, Yakopcic C, Taha TM. 3D memristor crossbar architecture for a multicore neuromorphic system. In: 2020 International Joint Conference on Neural Networks (IJCNN); 2020 Jul 19-24; Glasgow, UK. IEEE; 2020. p. 1-8. DOI
89. Ismail M, Chand U, Mahata C, Nebhen J, Kim S. Demonstration of synaptic and resistive switching characteristics in W/TiO<sub>2</sub>/HfO<sub>2</sub>/Ta<sub>2</sub>N memristor crossbar array for bioinspired neuromorphic computing. *J Mater Sci Technol* 2022;96:94-102. DOI
90. Balakrishna Pillai P, De Souza MM. Nanoionics-based three-terminal synaptic device using zinc oxide. *ACS Appl Mater Interfaces* 2017;9:1609-18. DOI PubMed
91. Lenz J, Del Giudice F, Geisenhof FR, Winterer F, Weitz RT. Vertical, electrolyte-gated organic transistors show continuous operation in the MA cm<sup>-2</sup> regime and artificial synaptic behaviour. *Nat Nanotechnol* 2019;14:579-85. DOI PubMed
92. Lee H, Cho SW, Kim SJ, et al. Three-terminal ovonic threshold switch (3T-OTS) with tunable threshold voltage for versatile artificial sensory neurons. *Nano Lett* 2022;22:733-9. DOI PubMed
93. Cohen MH, Fritzsche H, Ovshinsky SR. Simple band model for amorphous semiconducting alloys. *Phys Rev Lett* 1969;22:1065-8. DOI
94. Street RA, Mott NF. States in the gap in glassy semiconductors. *Phys Rev Lett* 1975;35:1293-6. DOI
95. Nakano M, Shibuya K, Okuyama D, et al. Collective bulk carrier delocalization driven by electrostatic surface charge accumulation. *Nature* 2012;487:459-62. DOI PubMed
96. Sarkar T, Lieberth K, Pavlou A, et al. An organic artificial spiking neuron for in situ neuromorphic sensing and biointerfacing. *Nat Electron* 2022;5:774-83. DOI
97. Parr ZS, Rashid RB, Paulsen BD, et al. Semiconducting small molecules as active materials for p-type accumulation mode organic electrochemical transistors. *Adv Elect Mater* 2020;6:2000215. DOI
98. Hidalgo Castillo TC, Moser M, Cendra C, et al. Simultaneous performance and stability improvement of a p-type organic electrochemical transistor through additives. *Chem Mater* 2022;34:6723-33. DOI
99. Sun H, Gerasimov J, Berggren M, Fabiano S. n-Type organic electrochemical transistors: materials and challenges. *J Mater Chem C* 2018;6:11778-84. DOI
100. Giovannitti A, Nielsen CB, Sbircea DT, et al. N-type organic electrochemical transistors with stability in water. *Nat Commun* 2016;7:13066. DOI PubMed PMC
101. Liu L, Xu W, Ni Y, et al. Stretchable neuromorphic transistor that combines multisensing and information processing for epidermal gesture recognition. *ACS Nano* 2022;16:2282-91. DOI PubMed
102. Imai J, Katagiri H. Regulation of systemic metabolism by the autonomic nervous system consisting of afferent and efferent innervation. *Int Immunol* 2022;34:67-79. DOI PubMed
103. Johansson RS, Flanagan JR. Coding and use of tactile signals from the fingertips in object manipulation tasks. *Nat Rev Neurosci* 2009;10:345-59. DOI PubMed
104. Wang W, Jiang Y, Zhong D, et al. Neuromorphic sensorimotor loop embodied by monolithically integrated, low-voltage, soft e-skin.



- Science* 2023;380:735-42. DOI PubMed
105. Liu F, Deswal S, Christou A, Sandamirskaya Y, Kaboli M, Dahiya R. Neuro-inspired electronic skin for robots. *Sci Robot* 2022;7:eabl7344. DOI PubMed
  106. Torricelli F, Adrahtas DZ, Bao Z, et al. Electrolyte-gated transistors for enhanced performance bioelectronics. *Nat Rev Method Prime* 2021;1:65. DOI
  107. Huang Y, Fan X, Chen S, Zhao N. Emerging technologies of flexible pressure sensors: materials, modeling, devices, and manufacturing. *Adv Funct Mater* 2019;29:1808509. DOI
  108. Kim Y, Chortos A, Xu W, et al. A bioinspired flexible organic artificial afferent nerve. *Science* 2018;360:998-1003. DOI PubMed
  109. Yao X, Zhang Y, Jin W, Hu Y, Cui Y. Carbon nanotube field-effect transistor-based chemical and biological sensors. *Sensors* 2021;21:995. DOI PubMed PMC
  110. Kim S, Lee Y, Kim H, Choi S. A tactile sensor system with sensory neurons and a perceptual synaptic network based on semivolatile carbon nanotube transistors. *NPG Asia Mater* 2020;12:76. DOI
  111. Lee Y, Liu Y, Seo DG, et al. A low-power stretchable neuromorphic nerve with proprioceptive feedback. *Nat Biomed Eng* 2023;7:511-9. DOI
  112. He Y, Zhu L, Zhu Y, et al. Recent progress on emerging transistor-based neuromorphic devices. *Adv Intell Syst* 2021;3:2000210. DOI
  113. Wang R, Sun L, Zhu X, et al. Carbon nanotube-based strain sensors: structures, fabrication, and applications. *Adv Mater Technol* 2023;8:2200855. DOI
  114. Ahuja P, Akiyama S, Ujjain SK, et al. A water-resilient carbon nanotube based strain sensor for monitoring structural integrity. *J Mater Chem A* 2019;7:19996-20005. DOI
  115. Karimov KS, Khalid FA, Chani MTS. Carbon nanotubes based strain sensors. *Measurement* 2012;45:918-21. DOI
  116. Kang SK, Murphy RKJ, Hwang SW, et al. Bioresorbable silicon electronic sensors for the brain. *Nature* 2016;530:71-6. DOI PubMed
  117. Kim DH, Viventi J, Amsden JJ, et al. Dissolvable films of silk fibroin for ultrathin conformal bio-integrated electronics. *Nat Mater* 2010;9:511-7. DOI PubMed PMC
  118. Song E, Li R, Jin X, et al. Ultrathin trilayer assemblies as long-lived barriers against water and ion penetration in flexible bioelectronic systems. *ACS Nano* 2018;12:10317-26. DOI PubMed
  119. Song E, Lee YK, Li R, et al. Transferred, ultrathin oxide bilayers as biofluid barriers for flexible electronic implants. *Adv Funct Mater* 2018;28:1702284. DOI
  120. Lee YK, Yu KJ, Song E, et al. Dissolution of monocrystalline silicon nanomembranes and their use as encapsulation layers and electrical interfaces in water-soluble electronics. *ACS Nano* 2017;11:12562-72. DOI PubMed PMC
  121. Kang SK, Koo J, Lee YK, Rogers JA. Advanced materials and devices for bioresorbable electronics. *Acc Chem Res* 2018;51:988-98. DOI PubMed
  122. Shin J, Yan Y, Bai W, et al. Bioresorbable pressure sensors protected with thermally grown silicon dioxide for the monitoring of chronic diseases and healing processes. *Nat Biomed Eng* 2019;3:37-46. DOI PubMed
  123. Boukhvalov DW, Nappini S, Vorokhta M, et al. Revisiting the chemical stability of germanium selenide (GeSe) and the origin of its photocatalytic efficiency. *Adv Funct Mater* 2021;31:2106228. DOI